COMPARISON BETWEEN PSEUDO-SPECTRAL TIME DOMAIN AND DISCRETE DIPOLE APPROXIMATION SIMULATIONS FOR SINGLE-SCATTERING PROPERTIES OF PARTICLES

A Thesis

by

DEREK IAN PODOWITZ

Submitted to the Office of Graduate Studies of
Texas A&M University
in partial fulfillment of the requirements for the degree of

MASTER OF SCIENCE

Chair of Committee,	Ping Yang
Committee Members,	George Kattawar
	R. Lee Panetta
	Gerald North
Head of Department,	Ping Yang

August 2013

Major Subject: Atmospheric Sciences

Copyright 2013 Derek Ian Podowitz

ABSTRACT

The pseudo-spectral time domain (PSTD) and discrete dipole approximation (DDA) are two of the most popular methods to model the single-scattering properties of ice crystals and aerosols. Both methods solve for Maxwell's equations. The PSTD method uses a Fourier pseudo-spectral method and a finite-difference method to compute the spatial and temporal derivatives of electromagnetic fields. The DDA method uses an electromagnetic integral equation in the frequency domain to calculate the single-scattering properties. We used a spherical model for this study because the analytical solution was given by the Lorenz-Mie theory. Previous studies have found that at refractive indices between 1.2 and 1.5, PSTD computed the single-scattering properties of spherical particles faster for large size parameters, while DDA was more computationally efficient at small size parameters; however, these previous studies did not consider absorptive cases. The purpose of this study was to expand the range of refractive indices to include absorptive cases and to determine which method was more efficient for computing the single-scattering properties of atmospheric particles within set criteria. The PSTD and DDA methods were systematically assessed in this study for 31 different realistic complex refractive indices. Similar to the previous studies, it was found that PSTD was more efficient than DDA for particles with large size parameters. The results in this study were consistent with the previous studies for non-absorptive to moderately absorptive particles. However, for strongly absorptive cases, DDA was more efficient than PSTD at all size parameters for the absorptive particles. It was also determined that the efficiencies of the two methods were dependent on both the real and imaginary parts of the complex refractive index. The significance of this study was to

improve our understanding of the capabilities of the PSTD and DDA methods for computing single-scattering properties.

ACKNOWLEDGEMENTS

I would like to thank my committee members Dr. Ping Yang, Dr. George Kattawar, Dr. R. Lee Panetta, and Dr. Gerald North. I would also like to thank Chao Liu for all his help and guidance throughout my research project. The reported research was partly supported by NSF (ATM-0803779) and NASA (NNX11AK37G), and the endowment funds related to the David Bullock Harris Chair in Geosciences at the College of Geosciences, Texas A&M University. All computations were carried out at the Texas A&M University Supercomputing Facility. Lastly, I would like to thank my family and friends for all their love and support through the years.

NOMENCLATURE

PSTD:	Pseudo-spectral time domain
(A)DDA:	(Amsterdam) discrete dipole approximation
E:	Electric field vector
H:	Magnetic field vector
Q_{ext}:	Extinction efficiency
$\widetilde{\omega}$:	Single-scattering albedo
g:	Asymmetry factor
P:	Phase matrix
RE:	Relative error
RMSRE:	Root mean square relative error

TABLE OF CONTENTS

LIST OF FIGURES

LIST OF TABLES

CHAPTER I

INTRODUCTION AND LITERATURE REVIEW

A variety of numerical methods have been used to compute single-scattering properties of different types of particles. The two methods that are assessed for this study are the pseudo-spectral time domain (PSTD) method and the discrete dipole approximation (DDA) method. Many studies have been done for the PSTD and DDA methods to assess their accuracies and computational efficiencies. The objective of this study is to systematically assess the accuracy and computational efficiency of these two methods for a wide range of realistic refractive indices of atmospheric particles. By considering realistic ice particle refractive indices, we can improve our understanding of the capabilities of the two numerical methods. Before we go into detail about the PSTD and DDA methods used in this study, we must first provide a background for computing single-scattering properties.

Light scattering models

Calculations for single-scattering properties can be done for many different types and shapes of particles. The simplest particle that single-scattering properties are computed for is the homogeneous sphere. A homogeneous sphere was used as the test particle in this study, because the analytical solution chosen for this study was the Lorenz-Mie theory.

Analytical solution: Lorenz-Mie theory

The Lorenz-Mie theory computes the single-scattering properties for spherical particles by using Maxwell's equations for electromagnetic fields. The electromagnetic wave equation for Lorenz-Mie theory is derived for a homogeneous particle where the permittivity and magnetic permeability are constant and the field has no charges or currents. The analysis

of the incident wave equation used to determine the formal scattering solution is done in spherical coordinates. The parallel and perpendicular components of the scattering electric field vectors are used to determine the phase matrix computed from Lorenz-Mie scattering (Mie 1908, Liou 2002).

Single-scattering properties

The phase matrix transforms the incident Stokes vector into the scattering Stokes vector. The Stokes vector indicates the properties of light in a system and is defined by four quantities known as the Stokes parameters. The 4 Stokes parameters are: irradiance or intensity of light (I); the irradiance with respect to a reference frame for linearly perpendicular and parallel polarized light (Q); the irradiance with respect to a reference frame for linearly polarized light at 45^{o} (U); and, circularly or elliptically polarized light (V) (Van du Hulst 1981). The Stokes parameters are determined from the equations below:

$$I = E_l E_l^* + E_r E_r^* \tag{1}$$

$$Q = E_l E_l^* - E_r E_r^* \tag{2}$$

$$U = E_l E_r^* + E_r E_l^* \tag{3}$$

$$V = -i(E_l E_r^* + E_r E_l^*), \tag{4}$$

where E_l^* is the complex conjugate of the parallel electric field, E_r^* is the complex conjugate of the perpendicular electric field, and $i = \sqrt{-1}$ (Liou 2002). The incident Stokes vector multiplied by the phase matrix is proportional to the scattering Stokes vector, and is defined by the following setup:

$$\begin{bmatrix} I_s \\ Q_s \\ U_s \\ V_s \end{bmatrix} \propto \mathbf{P} \begin{bmatrix} I_i \\ Q_i \\ U_i \\ V_i \end{bmatrix}, \tag{5}$$

where **P** is the phase matrix and the *i* and *s* subscripts indicate the incident and scattering Stokes parameters. The phase matrix for a single homogeneous sphere is given as:

$$\mathbf{P} = \begin{bmatrix} P_{11} & P_{12} & 0 & 0 \\ P_{12} & P_{11} & 0 & 0 \\ 0 & 0 & P_{33} & P_{34} \\ 0 & 0 & -P_{34} & P_{33} \end{bmatrix}, \quad (6)$$

where P_{11}, P_{12}, P_{33}, and P_{34} represent the components or elements of the phase matrix. For a phase matrix calculated by the Lorenz-Mie theory, eight of the sixteen components remain and the phase elements for P_{21}, P_{22}, P_{43}, and P_{44} are equivalent to P_{12}, P_{11}, -P_{34}, and P_{34}, respectively. The P_{11} component is also known as the phase function (Mie 1908, Liou 2002).

In addition to the phase matrix, light scattering models also compute the extinction efficiency (Q_{ext}), the single-scattering albedo ($\tilde{\omega}$), and the asymmetry factor (g). The extinction efficiency (Q_{ext}) represents how well a particle absorbs or scatters light (Liou 2002). The size parameter ($x = (2\pi \cdot r)/\lambda$) of a particle is a unitless variable that represents the relationship between a particle's radius and the wavelength inside the particle (Thomas and Stamnes 1999). Physically, the imaginary part (m_i) represents the amount of absorption of light that passes through the particle. If $m_i = 0$, there is no absorption, and if $m_i = 1$, the particle completely absorbs the light. The single-scattering albedo is the ratio of the scattering efficiency to the extinction efficiency. The ratio helps to assess how well a particle absorbs light. The absorptivity of a particle affects the phase functions and the efficiencies of the particle to stop or scatter light passing through the particle. The asymmetry factor (g) is a ratio from -1 to 1 which represents degree of the asymmetry of the angular scattering by a particle (Thomas and Stamnes 1999). If g = -1, a particle completely backscatters light; if g = 1, a particle completely forward scatters light; and, if g = 0, a

particle scatters light equally in as directions. The Q_{ext}, $\tilde{\omega}$, and g are values that can be used to validate light scattering models.

The Lorenz-Mie theory was used to validate the accuracy of the two numerical methods, PSTD and DDA, analyzed for this study. In order to verify the accuracy of PSTD and DDA, the errors between the numerical solutions and the analytical solution are calculated for Q_{ext} and the P_{11} phase function. These error calculations will be addressed in the methods and data section of this paper.

Numerical methods for computing single-scattering properties

The two numerical methods used to calculate the single-scattering properties of the modeled spherical particles for this study are the pseudo-spectral time domain (PSTD) and discrete dipole approximation (DDA). These two methods will be compared to and validated by the Lorenz-Mie theory.

Pseudo-spectral time domain method

The pseudo-spectral time domain method is a high-order approximation that uses a coarse grid resolution based on a spectral method to solve Maxwell's equations. PSTD uses a second-order finite difference to compute the time derivative and has similar conversion methods as the Finite Difference Time Domain (FDTD) method (Liu et al. 2012a, Yang and Liou 1996). Figure 1 represents the grid-space environment that the spherical test particle is located in and describes the computational domain of PSTD. PSTD calculates the components of electromagnetic field in the center of each grid-space. The environment shown in Figure 1 includes the initial wave of light begins at a point within the computational domain and region between orange and blue rectangle boundaries is known as the perfectly

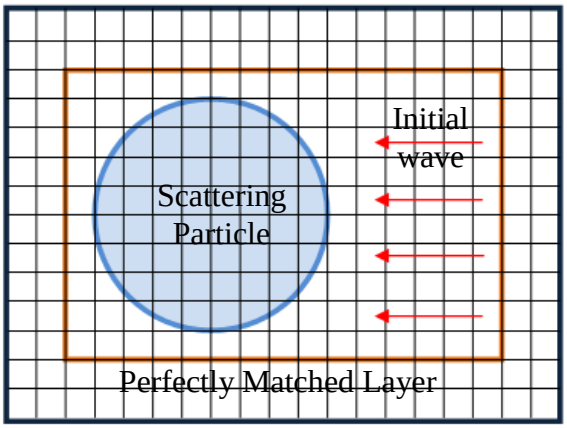

Figure 1 A cross-section of a test particle placed in the grid-space environment (based on Figure 1a of Yang and Liou 2000).

matched layer (PML). The PML condition employs an absorbing medium outside the computational domain of the theoretical particle in order to absorb outgoing waves scattered by the particle (Chen 2007). The PSTD method differs from FDTD when computing the spatial derivative.

PSTD's spatial derivative is computed by taking the inverse fast Fourier transformation (IFFT) of the spectral coefficients which are computed by the FFT multiplied by coefficients ($2\pi k_l i$) and a filter (σ(η)). The spatial derivative of PSTD is represented by the following equation (Liu et al. 2012a):

$$\frac{\partial F^n(I,J,K)}{\partial x} = \frac{1}{N}\sum_{l=-N/2}^{\frac{N}{2}-1} e^{((2\pi Il)/N)i}\left[2\pi k_l i * \sigma(\eta) * \sum_{m=1}^{N} F^n(m,J,K)e^{-\left(\frac{2\pi lm}{N}\right)i}\right], \quad (7)$$

where I, J, and K represent the components of the grid space shown in Figure 1b, N is the number of grid-spaces used to represent the particle shape, and n is the iteration number.

Filters, represented by σ(η) in Equation 7, are introduced to the PSTD method in order to reduce Gibb's phenomenon. Gibb's phenomenon is the occurrence of oscillations due to a numerical method's attempt at approximating discontinuous points along a given

function. PSTD is capable of using different types of filters; however, most studies have used the truncation filter. The filter used in this study was a truncation filter. The relationship for the truncation filter is as follows:

$$\sigma(\eta) = \begin{cases} 0 & |\eta| > \eta_c \\ 1 & |\eta| \leq \eta_c \end{cases}. \quad (8)$$

The truncation filter uses a constant ratio (η_c) as the criteria for truncating the data. The $|\eta|$ ratio is represented by taking the absolute value the iteration number (n) divided by one-half the number of grid-spaces (l). The data points are removed for values of $|\eta|$ greater than η_c and are kept for values of $|\eta|$ less than or equal to η_c. The truncation ratio represents the percentage of data that is filtered out to correct for PSTD's approximation of phase functions (Hesthaven et al. 2007).

For this study the pseudo-spectral time domain method used scheme 1 from Chen's 2007 PhD. dissertation to approximate single-scattering properties of spherical particles. The following terms are computed and used for scheme 1: $\boldsymbol{E}^s$ is the scattered electric field vector; $\boldsymbol{H}^s$ is the scattered magnetic field vector; ε_0 is the permittivity in a vacuum; $\bar{\varepsilon}_r$ is the real part of the permittivity; $\bar{\varepsilon}_i$ is the imaginary part of the permittivity; k is the wavenumber of incident radiation; c is the speed of light; and, n is the step number. $\boldsymbol{E}^s$, $\boldsymbol{H}^s$, $\bar{\varepsilon}_r$, and $\bar{\varepsilon}_i$ are dependent on I, J, and K for the iteration, but have been removed for clarity from the set of equations below (9-17) for the scheme of this method. The equations below represent the x-component of the electric field; the y and z components follow the same scheme.

Equation 9 represents the calculated iterations for computing the scattering electric field vector, and equation 9 is dependent on variables computed in Equations 10 through 17. In this study, the scheme used for PSTD is as follows:

$$\int_{n\Delta t}^{(n+1)\Delta t}\left\{\varepsilon_0\bar{\varepsilon}_r\frac{\partial E_x^s}{\partial t}+kc\varepsilon_0\bar{\varepsilon}_i E_x^s\right\}dt = \tag{9}$$

$$\int_{n\Delta t}^{(n+1)\Delta t}\left\{\frac{\partial H_z^s}{\partial y}-\frac{\partial H_y^s}{\partial z}\right\}dt+\int_{n\Delta t}^{(n+1)\Delta t}\left\{\varepsilon_0(1-\bar{\varepsilon}_r)\frac{\partial E_x^i}{\partial t}+kc\varepsilon_0\bar{\varepsilon}_i E_x^i\right\}dt$$

$$\bar{\varepsilon}_r=\frac{\int_{(I-1)\Delta x}^{I\Delta x}\int_{(J-1)\Delta y}^{J\Delta y}\int_{(K-1)\Delta z}^{K\Delta z}\varepsilon_r(x,y,z)dxdydz}{\Delta x\Delta y\Delta z} \tag{10}$$

$$\bar{\varepsilon}_i=\frac{\int_{(I-1)\Delta x}^{I\Delta x}\int_{(J-1)\Delta y}^{J\Delta y}\int_{(K-1)\Delta z}^{K\Delta z}\varepsilon_i(x,y,z)dxdydz}{\Delta x\Delta y\Delta z} \tag{11}$$

$$\int_{n\Delta t}^{(n+1)\Delta t}\frac{\partial E_x^s}{\partial t}dt=E_x^{s(n+1)}-E_x^{s(n)} \tag{12}$$

$$\int_{n\Delta t}^{(n+1)\Delta t}E_x^s dt=\frac{\Delta t}{2}((E_x^{s(n+1)}-E_x^{s(n)}) \tag{13}$$

$$\int_{n\Delta t}^{(n+1)\Delta t}\frac{\partial E_x^i}{\partial t}dt=\frac{\partial E_x^{i(n+1/2)}}{\partial t} \tag{14}$$

$$\int_{n\Delta t}^{(n+1)\Delta t}E_x^i dt=\Delta t E_x^{i(n+1/2)} \tag{15}$$

$$\int_{n\Delta t}^{(n+1)\Delta t}\frac{\partial H_z^s}{\partial y}dt=\frac{\partial H_z^{s(n+1/2)}}{\partial y} \tag{16}$$

$$\int_{n\Delta t}^{(n+1)\Delta t}\frac{\partial H_y^s}{\partial z}dt=\frac{\partial H_y^{s(n+1/2)}}{\partial z}. \tag{17}$$

The pseudo-spectral time domain method used for this study uses the scheme presented above to approximate light scattering properties of the spherical ice particles. PSTD is the first of the two numerical methods used in this study for comparing computations of spherical ice particles to Lorenz-Mie theory. The second numerical method assessed in this study was the discrete dipole approximation method.

Discrete dipole approximation method

The discrete dipole approximation (DDA) was developed to simulate single-scattering properties of particles by calculating their ability to scatter and absorb

electromagnetic waves (Yurkin and Hoekstra 2011). DDA uses the solution of a linear system to determine unknown dipole polarizations:

$$E_i^{inc} = \bar{\alpha}_i{}^{-1} P_i - \sum_{j \neq 1} \bar{G}_{ij} P_j, \quad (18)$$

where E^{inc} is the incident electric field, α is the dipole polarizability, G is a Green's function known as the interaction term, and P is the polarization. The interaction term and polarization values are dependent on the number of dipoles used to model a test particle. Once the polarizations and interaction terms are determined, the single-scattering properties can be computed (Yurkin and Hoekstra 2011).

The code for DDA simulations have been modified and corrected by Hoekstra, Yurkin, and their teams at University of Amsterdam. Their version of the code was named Amsterdam DDA or ADDA. From this point forward the ADDA notation will be used when comparing this method numerically to PSTD and the Lorenz-Mie theory. The ADDA method uses a grid-spacing method similar to PSTD to compute the values of the electromagnetic fields that determine the single-scattering properties of a spherical particle. The particle computed by ADDA is represented by point dipoles (Yurkin and Hoekstra 2011). A point dipole is a dipole that is located at a point inside a three dimensional grid-space. The setup for the ADDA particle environment is similar to the environment shown in Figure 1, but it does not include the PML condition (Yurkin et al. 2007). The number of dipoles present in the particle represents the spatial resolution for the ADDA simulations (Yurkin and Hoekstra 2009). Now that we have introduced the PSTD and ADDA methods, we will discuss the procedure of this study in the next section.

CHAPTER II

METHODOLOGY

Methods and data

This study assessed non-absorptive and absorptive cases of complex refractive indices for spherical particles. The Lorenz-Mie theory computes the single-scattering properties of spherical particles. Spherical particles were used for this study because the Lorenz-Mie was used as our analytical solution for comparing the computational accuracies and times of PSTD and DDA. We modeled single-scattering properties of spheres using codes for PSTD and DDA methods and compare the values to the Lorenz-Mie theory solution for 31 different wavelengths between 0.2 μm and 100 μm and eight size parameters (x) from 5 to 100. Figures 2a and 2b represent the 31 wavelengths used to assess the comparison between the analytical solution and the two numerical methods used to approximate the solutions of the single-scattering properties of spherical particles. Figure 2a displays the all the data from the Warren and Brandt 2008 dataset. The blue points on this figure are the data points chosen for this study. Figure 2b shows how the three cases are grouped together; the magenta data points represent case 1 data, the blue data points represent case 2 data, and the green data points represent case 3 data. The dashed red lines on the m_i versus wavelength graph in Figure 2b represent the boundaries of the case ranges mentioned previously.

Table 1 displays the numerical values used in this for the wavelengths and their respective complex refractive indices separated into 4 cases. Thirty of the wavelengths are split into 3 separate cases, where the real part of the refractive index (m_r) varied between 0.954 and 1.870. The three cases divided the wavelengths into categories based on their

imaginary refractive indices. The first case represented 10 wavelengths with non-absorptive refractive indices. What constituted a non-absorptive or weakly absorptive case was that the imaginary refractive index (m_i) was less than 10^{-3}. The second case represented 10 moderately absorptive wavelengths where $10^{-3} < m_i < 10^{-1}$. The third case represented 10 strongly absorptive wavelengths where m_i is greater than 10^{-1}. The data in each case represented a wide range of wavelengths from visible to microwave wavelengths. Most of the data in Case 1 represent wavelengths in the visible and near-infrared. Cases 2 and 3 had a few overlapping wavelengths in the infrared and microwave wavelength ranges. The 31st data point had a wavelength larger than 100 μm, and was chosen to represent a microwave wavelength case with a large real refractive index and a weak to moderate absorption. This extra wavelength demonstrated the difference between the other cases with similar large real refractive indices, but with decreasing imaginary refractive indices.

As mentioned previously, the phase matrices of 8 different size parameters (x) at each of the 31 wavelengths were calculated by PSTD and ADDA simulations and then validated by the Lorenz-Mie theory. The 8 size parameters chosen for this study were x = {5, 10, 20, 30, 40, 60, 80, 100}. This size parameter range was selected in order to show the accuracies and computational efficiencies of PSTD versus ADDA at both small and large values of x. In order to appropriately compare PSTD and ADDA, we created a set of criteria for our study.

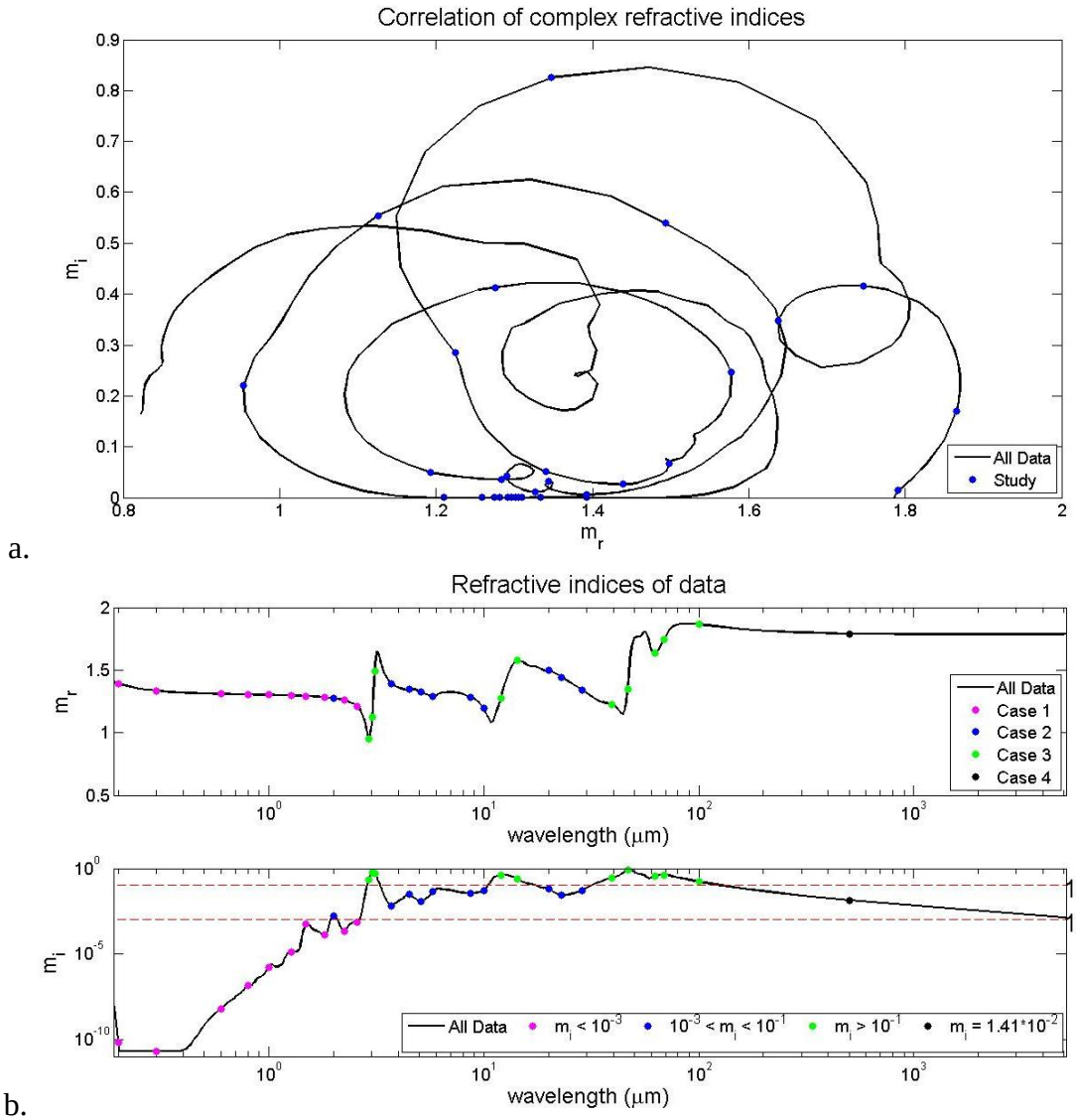

Figure 2 a. Data points used for study and their m_r and m_i correlations. b. Real (top) and imaginary (bottom) parts of the refractive indices with respect to wavelength for the 3 cases of this study. This data (in black) is from the Warren and Brandt 2008 data set for ice crystal refractive-indices.

Wavelengths and complex refractive indices used in study											
Case 1	λ (μm)	m_r	m_i	Case 2	λ (μm)	m_r	m_i	Case 3	λ (μm)	m_r	m_i (-1)
$m_i < 10^{-3}$	0.20	1.39	6.41(-11)	$m_i < 10^{-1}$ & $m_i > 10^{-3}$	2.00	1.27	1.64(-3)	$m_i > 10^{-1}$	2.92	0.95	2.21
	0.30	1.33	2.00(-11)		3.73	1.39	6.67(-3)		3.04	1.13	5.54
	0.60	1.31	5.73(-9)		4.51	1.34	3.18(-2)		3.12	1.49	5.39
	0.80	1.31	1.34(-7)		5.10	1.33	1.22(-2)		12.0	1.28	4.13
	1.00	1.30	1.62(-6)		5.81	1.29	4.27(-2)		14.3	1.58	2.46
	1.27	1.30	1.35(-5)		8.70	1.28	3.65(-2)		39.6	1.22	2.85
	1.49	1.29	5.53(-4)		10.0	1.19	5.01(-2)		46.7	1.35	8.25
	1.83	1.28	1.30(-4)		20.0	1.50	6.70(-2)		62.5	1.64	3.47
	2.25	1.26	2.03(-4)		23.1	1.44	2.70(-2)		69.0	1.75	4.17
	2.58	1.21	7.39(-4)		28.6	1.34	5.12(-2)		100	1.87	1.71
	Case 4				500	1.79	1.41(-2)				

Table 1 Selected wavelengths and complex refractive indices used for study. The above (#) notation represents the exponent in scientific notation ($10^{\#}$).

Validating methods

As previously mentioned in the introduction, we calculated the relative error (RE) of the extinction efficiency (Q_{ext}) and the root mean squared relative error (RMSRE) of the P_{11} phase function. The RE of Q_{ext} and RMSRE of P_{11} were used to assess the accuracy of PSTD and ADDA with respect to Lorenz-Mie theory (Yurkin et al. 2007). Our first task was to compute the extinction efficiency and the P_{11} phase functions within a certain percentage accuracy when compared to Lorenz-Mie theory. We wanted to have comparable accuracies between the PSTD and ADDA simulations, so that we could determine whether PSTD or ADDA was the better choice for specific computations using time as our deciding factor. The method with a faster computational efficiency at each size parameter and wavelength would be considered as the primary method that should be used when computing the single-scattering properties of the particles.

Criteria used

Criteria were chosen for the PSTD and ADDA to obtain similar accuracies to validate the numerical methods. These criteria were RE ≤ 2% for the Q_{ext} and RMSRE ≤ 30% for the P_{11} phase function when comparing each of the numerical simulations separately to the Lorenz-Mie theory (Liu et al. 2012b, Yurkin et al. 2007). Figure 3a shows the averages of the relative error of the extinction efficiency, and Figure 3b shows the averages of the root mean squared relative error of the P_{11} phase function for the 3 different cases. The averages shown in Figure 3 were computed by using the weighted average mean which removed any error values greater than 2% for the RE and 30% for the RMSRE. We modified the parameters related to the spatial resolution to refine the approximations and error calculations for the PSTD and ADDA methods.

Spatial resolution and computational time

PSTD and ADDA use different parameters to adjust their spatial resolutions. The parameter used to modify the spatial resolution for PSTD is the wavelength over the change in distance the light in the particle travels ($\lambda/\Delta x$). The $\lambda/\Delta x$ term uses the number of grid points or cells per wavelength to compute the spatial resolution (Liu et al. 2012a, Liu et al. 2012b). The ADDA code uses the parameter dipole per lambda (dpl) to modify the spatial resolution. The dpl is the number of dipoles per wavelength present within the particle and refines the shape of the approximated spherical particle. In order to meet the set criteria, the spatial resolution was increased; however, by increasing the spatial resolution the computational time would increase. Since computational time increased with increasing spatial resolution, time became a factor in deciding a numerical method's efficiency. The time limit chosen was 48 hours of total wall time. If the numerical method did not complete

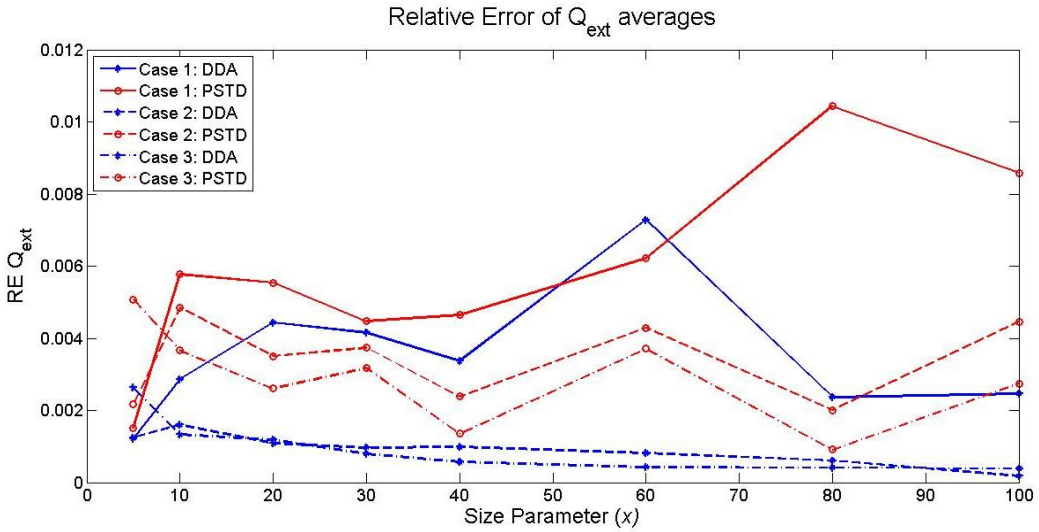

a.

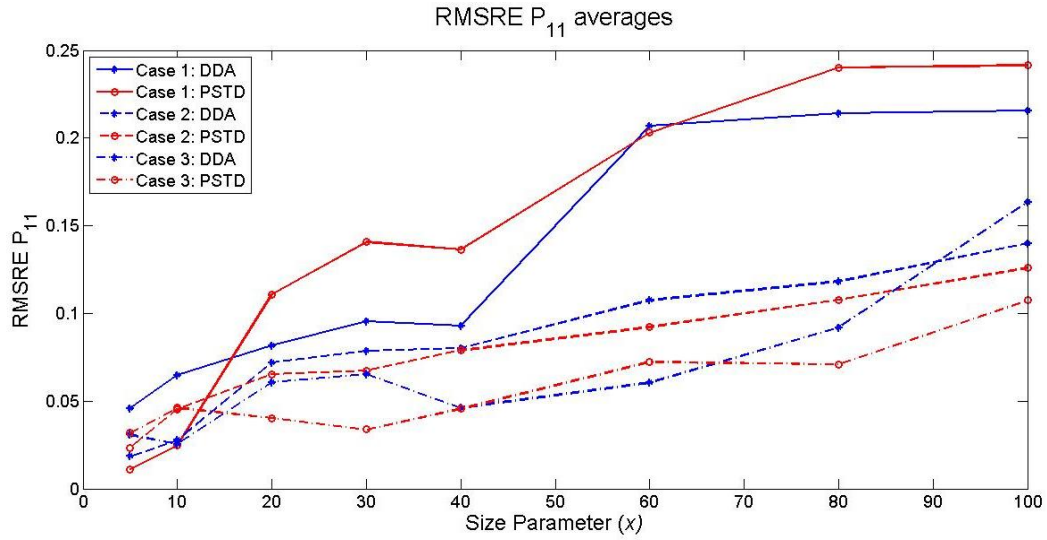

b.

Figure 3 a. Average relative error of Q_{ext} computed by PSTD and ADDA for the 3 cases. b. Average root mean squared relative error of the P_{11} phase function computed by PSTD and ADDA.

the run and converge within 48 hours running on a parallelization of 8 processors, then spatial resolution was modified or reduced to meet this time constraint. If a simulation continued to diverge upon reducing the spatial resolution parameters, we removed the size

parameter from our assessment. In addition to the computational time assessments for the 31 wavelengths, the phase matrices of these wavelengths were compared.

Phase matrix computation

Graphical analysis was used to compare the phase matrices computed by PSTD and ADDA to the phase matrix computed by the Lorenz-Mie theory. For the analysis of this study, the phase matrix elements were compared with respect to the scattering angle of the light (Yurkin et al. 2007). The graphs of the scattering phase matrix elements are the result of how light passing through a particle interacts with the structure of the particle. The phase matrices for a few absorptive and non-absorptive refractive indices from the 4 cases will be shown and assessed in the subsequent sections.

CHAPTER III

RESULTS

The single-scattering properties of atmospheric particles mathematically represent how light is affected by those particles when the light and atmospheric particles interact with each other. The data for this project represented a wide range of the particle sizes, wavelength bands, and refractive indices. PSTD and ADDA were the two numerical methods used to compute the single-scattering properties. The accuracies and computational times of these two methods were computed and compared through a series of steps.

Approach

The procedure to compare PSTD and ADDA to each other and to the Lorenz-Mie theory began with selecting the 31 wavelengths for the study which was done based on their complex refractive indices. At each wavelength, PSTD and ADDA were assessed at 8 different size parameters. At each size parameter, a spatial resolution was chosen and the simulations were run. If the criteria (RE $\leq$ 2%, RMSRE $\leq$ 30%) were met, the spatial resolution was kept and later refined depending on its computational time. If the criteria were not met, then the spatial resolution was adjusted accordingly. Once the spatial resolutions were finalized, the phase matrix analysis and computational time assessment were done for the 2 methods.

Phase matrix analysis

As previously stated in the methods and data section, the analysis of the phase matrices was done for a few examples. Only results for 3 of the 8 size parameters will be shown in order to keep the results concise. The three size parameters were 20, 60, and 100;

these represented a small size parameter, a moderate size parameter, and a large size parameter. Additionally, only one wavelength from each of the cases was chosen to represent the non-absorptive / weakly absorptive, moderately absorptive, and strongly absorptive cases that were assessed for this study. The wavelengths and refractive indices for these cases are shown below:

Wavelengths chosen to display and analyze phase matrices			
Case	Wavelength (μm)	m_r	m_i
1	0.60	1.31	$5.73 \cdot 10^{-9}$
2	3.73	1.39	$6.67 \cdot 10^{-3}$
3	12.0	1.28	$4.13 \cdot 10^{-1}$
4	500	1.79	$1.41 \cdot 10^{-2}$

Table 2 Four wavelengths used as examples for phase matrices results.

The fourth case had an imaginary refractive index similar to the weak absorption of Case 2, but the real refractive index was larger than the rest of the cases (1.79). As stated previously, we will examine 3 of the 8 size parameters for the 4 examples. Table 3 shows the spatial resolutions used to initialize the two computations of the single-scattering properties for the 4 examples.

Spatial resolutions of the numerical methods for the 4 example cases						
	$x = 20$		$x = 60$		$x = 100$	
Case	PSTD	ADDA	PSTD	ADDA	PSTD	ADDA
1	20	15	15	15	10	9
2	15	15	12	12	8	10
3	20	15	12	12	8	10
4	20	25	15	13	12	6

Table 3 Spatial resolutions of PSTD and ADDA that correspond to the 4 wavelengths in Table 2.

Figures 4 through 7 (on the subsequent pages) are plots of the phase matrix elements and their respective relative and absolute errors of the examples from Table 2. These phase matrix figures were plotted with respect to the scattering angle of light. In Figure 4, PSTD

and ADDA simulations correlate similarly to the Lorenz-Mie theory phase matrix elements. Figure 4a shows the PSTD method (red), the ADDA method (blue), and the Lorenz-Mie (black) theory phase matrix elements plots which contain the P_{11} phase functions, the P_{12}/P_{11} phase ratios which are the degree of linear polarization, the P_{33}/P_{11} phase ratios, and P_{34}/P_{11} phase ratios for Case 1 ($\lambda = 0.60$ μm, $m = 1.31+5.73\cdot10\text{-}9i$), Case 2 ($\lambda = 3.73$ μm, $m = 1.39+6.67\cdot10^{-3}i$), and Case 3 ($\lambda = 12.0$ μm, $m = 1.28+4.13\cdot10^{-1}i$) at size parameter $x = 20$. Figure 4b shows the relative error of the P_{11} phase functions, and the absolute errors of the P_{12}/P_{11}, P_{33}/P_{11}, and the P_{34}/P_{11} phase ratios for the 3 cases. Figure 5a and Figure 6a show the phase matrix elements for the 3 different cases, but for size parameters of $x = 60$ and $x = 100$, respectively. Just as in Figure 4b, Figure 5b and Figure 6b show the relative error and absolute errors for the phase matrix elements. For size parameter x = 60 and x = 100, in Figure 5, the PSTD and ADDA simulations become more variable with respect to the Lorenz-Mie theory than the simulations shown in Figure 4. In Figure 6, the phase matrix elements of PSTD and ADDA at x = 100 become even more variable and ADDA has less of a correlation to the Lorenz-Mie theory for the Case 1 and Case 2 plots. Figure 7a shows the phase matrix elements for Case 4 ($\lambda = 500$ μm, $m = 1.79+1.41\cdot10^{-2}i$) at $x = 20$ (left), $x = 60$ (center), $x = 100$ (right). Figure 7b shows the relative errors of the P_{11} phase functions and the absolute errors of P_{12}/P_{11}, P_{33}/P_{11}, and P_{34}/P_{11} ratios for the 3 size parameters of case 4. Figure 7 has similar increases in variability of the three size parameters to Figures 4 through 6. Further analyses and details of these figures will be done in the next chapter following the explanation of the computational times found in this study.

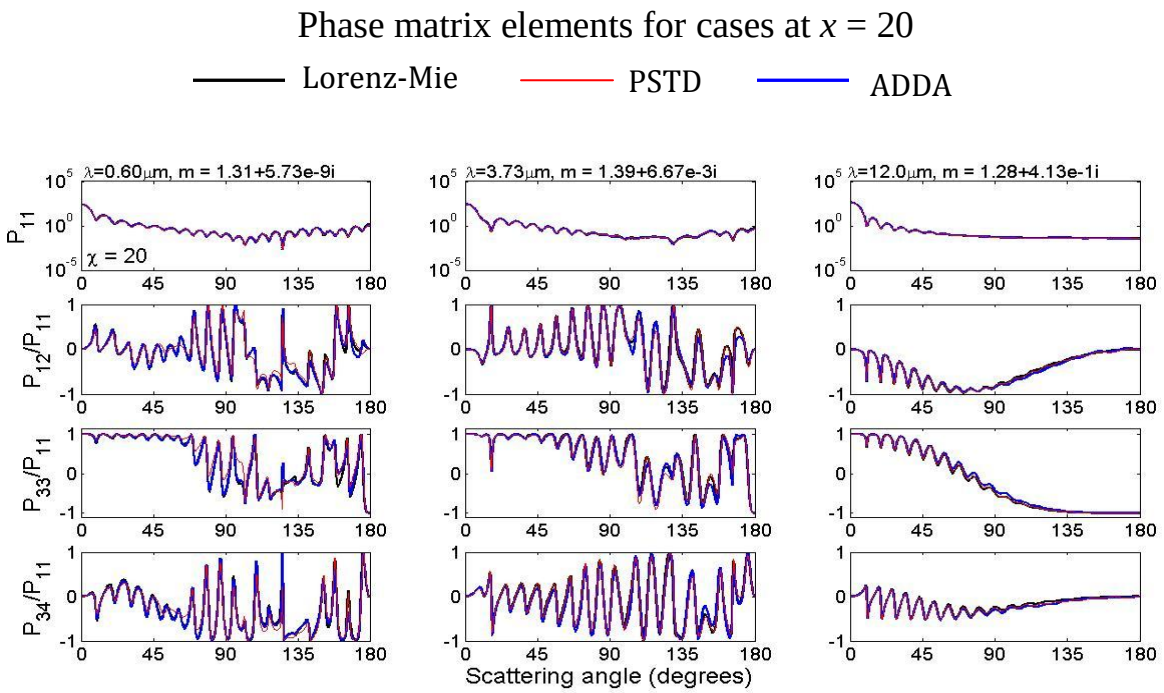

a.

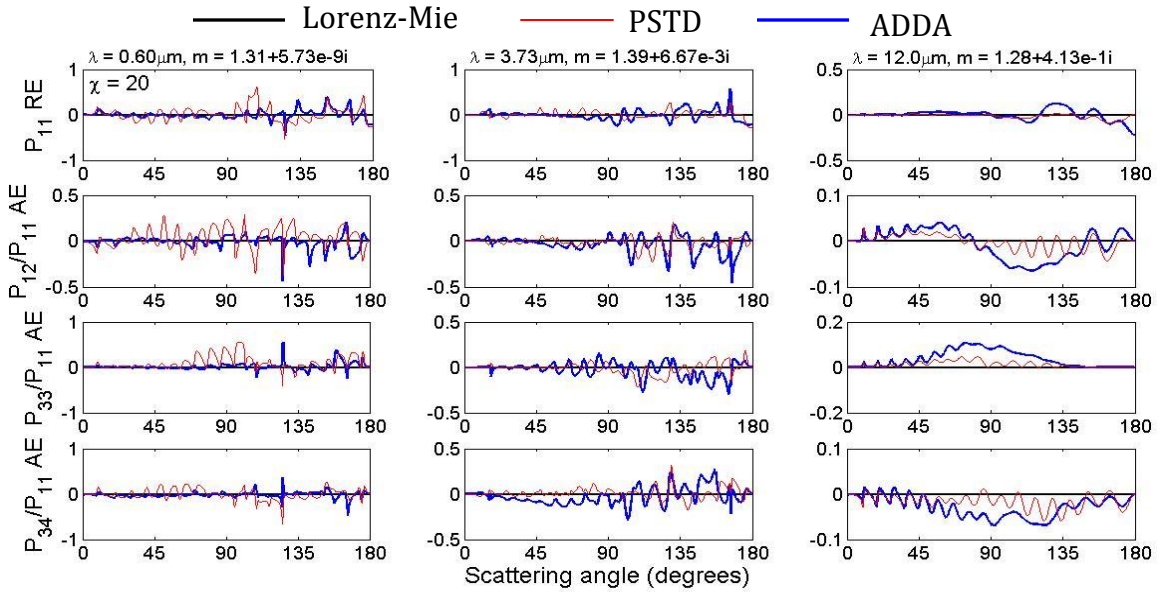

b.

Figure 4 a. Phase matrix elements of three different particles for a size parameter equal to 20. Each wavelength represents 1 example for each of the first 3 cases. b. Errors in the phase matrix elements computed by PSTD and ADDA of 3 wavelengths at $x = 20$.

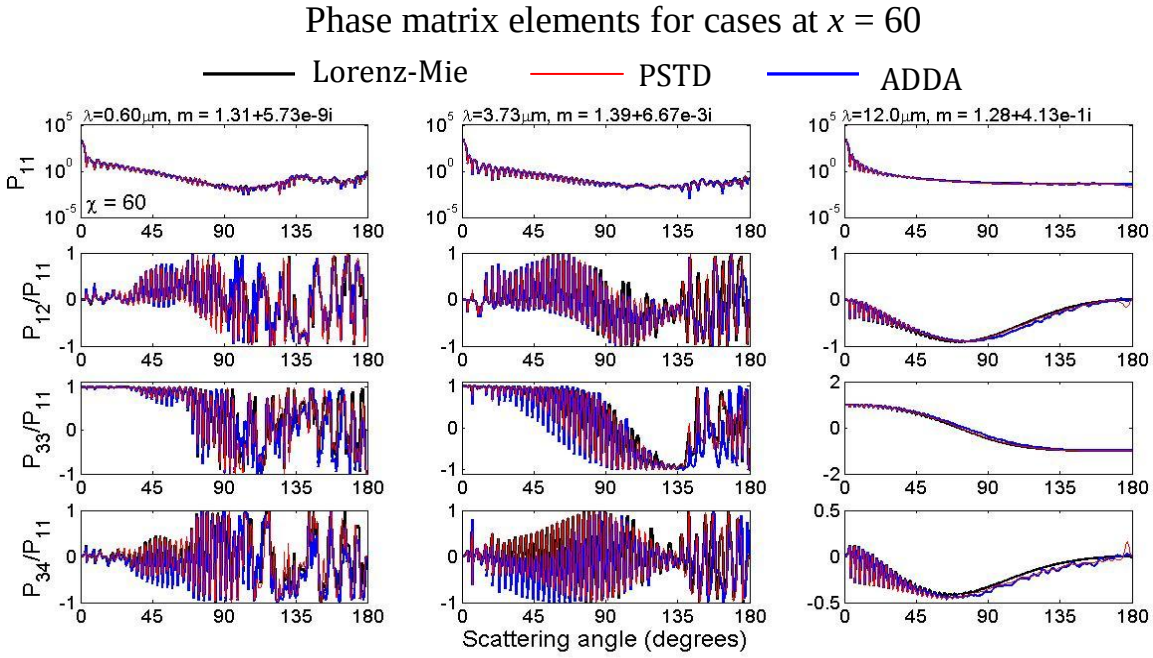

a.

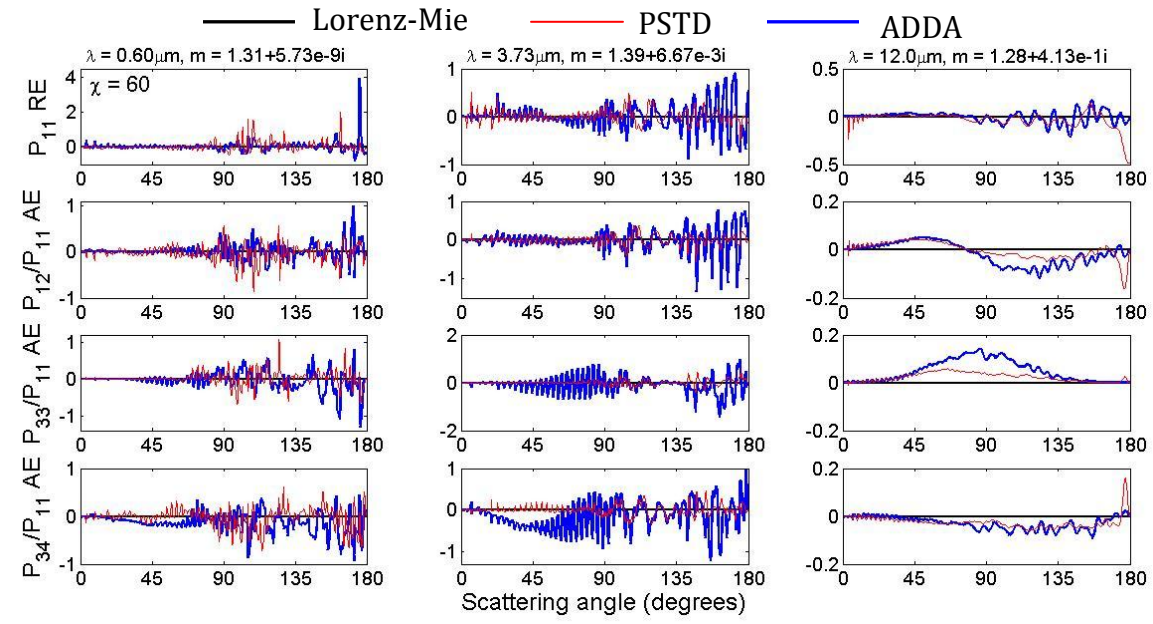

b.

Figure 5 a. Phase matrix elements of three different particles for a size parameter equal to 60. Each wavelength represents 1 example for each of the first 3 cases. b. Errors in the phase matrix elements computed by PSTD and ADDA of 3 wavelengths at $x = 60$.

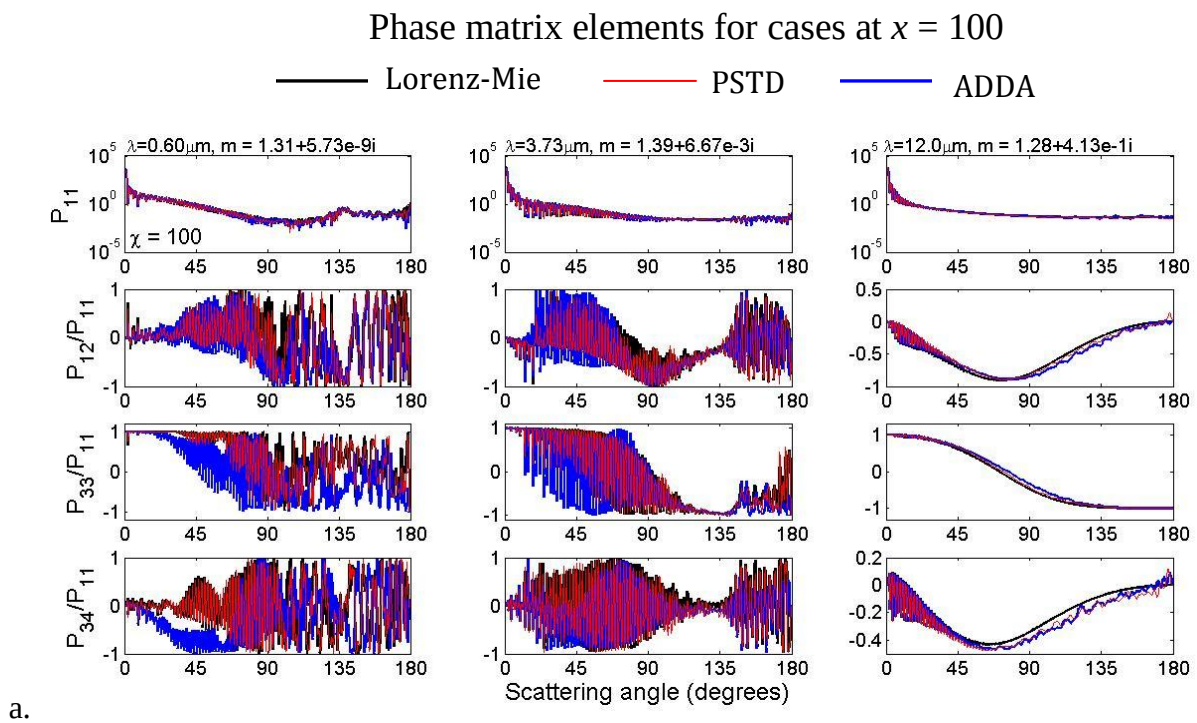

a.

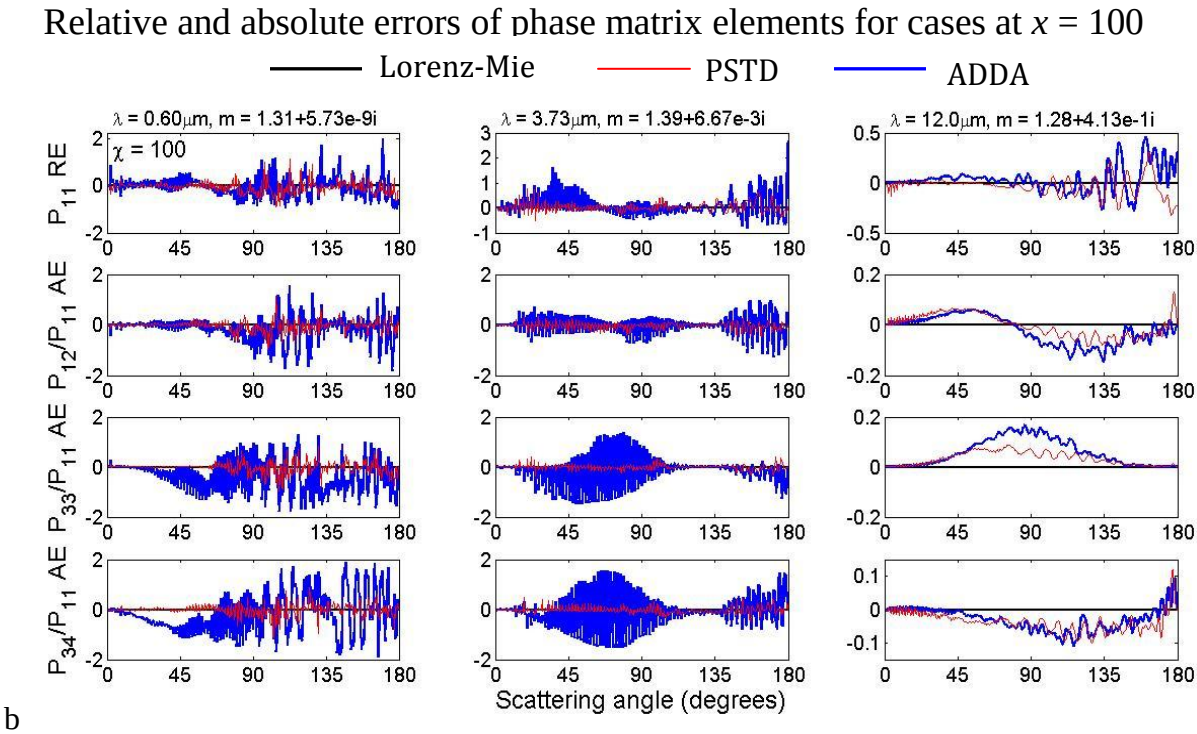

b

Figure 6 a. Phase matrix elements of three different particles for a size parameter equal to 100. Each wavelength represents 1 example for each of the first 3 cases. b. Errors in the phase matrix elements computed by PSTD and ADDA of 3 wavelengths at $x = 100$.

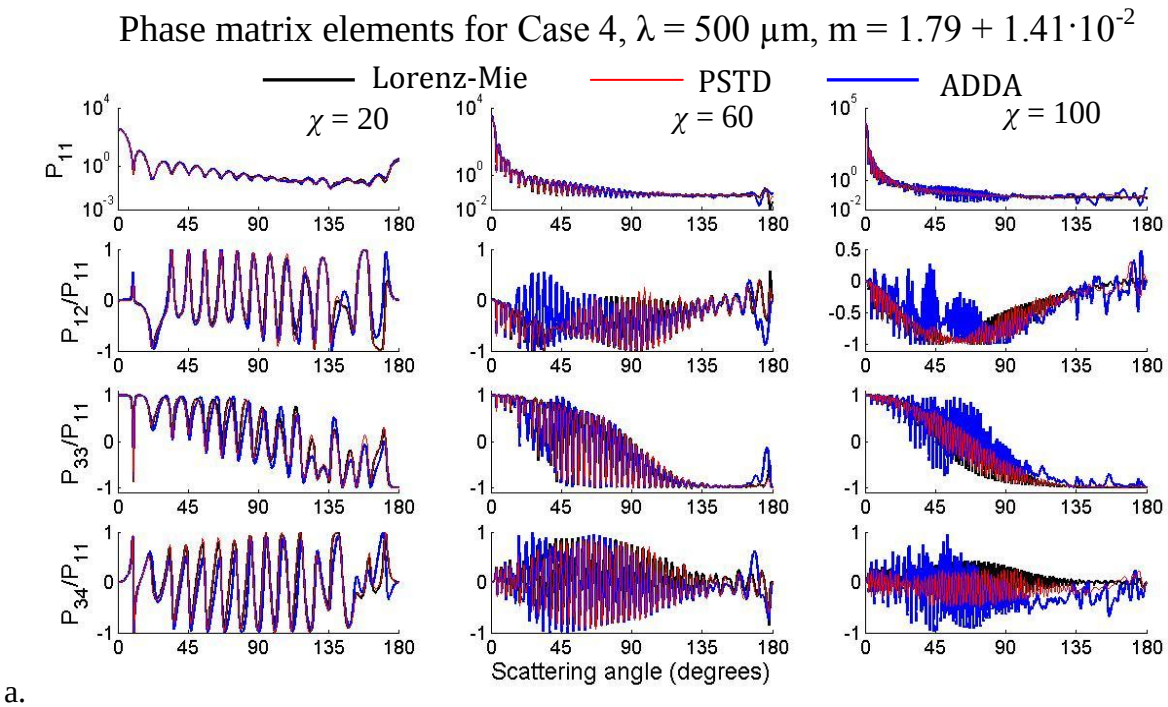

a.

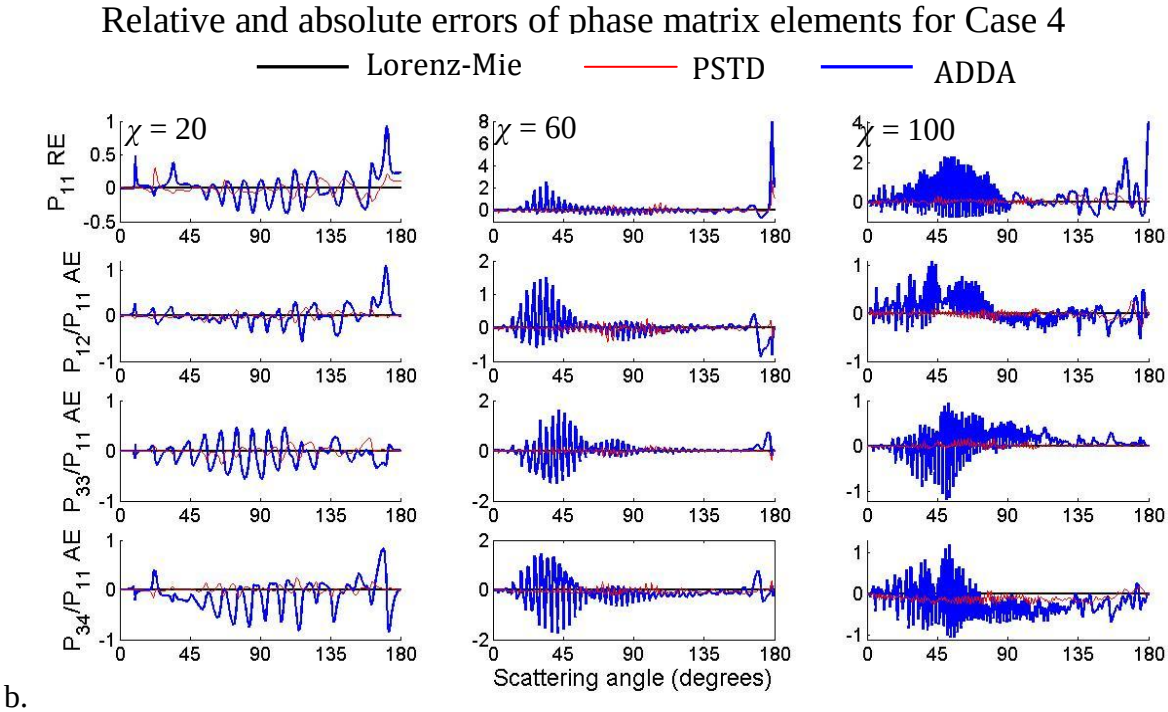

b.

Figure 7 a. Phase matrix elements for particles at 500 microns with 3 different size parameters (20, 60, 100) and a weak absorptive refractive index. b. Errors in the phase matrix elements computed by PSTD and ADDA for Case 4.

Computational time

The computational times of the PSTD and ADDA methods were compared with each for each wavelength and size parameter in order to determine which method was more efficient. Figure 8 shows the computational efficiency results for the wavelengths in Cases 1 through 3. In the figure, there is a point at each of the 8 size parameters, x = {5, 10, 20, 30, 40, 60, 80, 100}, for the 30 wavelengths. Each dot represented whether PSTD or ADDA was more efficient and whether or not both methods met the accuracy criteria of the study. The solid color dots meant that PSTD was more efficient than ADDA at computing the single-scattering properties and the white filled dots meant that ADDA was more efficient that PSTD. The green-colored dots signified that both numerical methods met the accuracy criteria. The red-colored dots signified that PSTD met both accuracy criteria, but ADDA only met one or neither criterion. The blue-colored dots shared the same conditions as the red dots, but ADDA was the method that met both accuracy criteria. The results of the computational time displayed on Figure 8 indicated that both PSTD and ADDA met the accuracy criteria for most of the data.

The computational time results for the fourth case were not displayed in Figure 8. Table 3 represents the raw data computational time results for this case. Table 3 and Figure 8 will be assessed in the discussion of this paper. The relationship between the computational time and the phase matrix analysis will also be discussed in the next chapter.

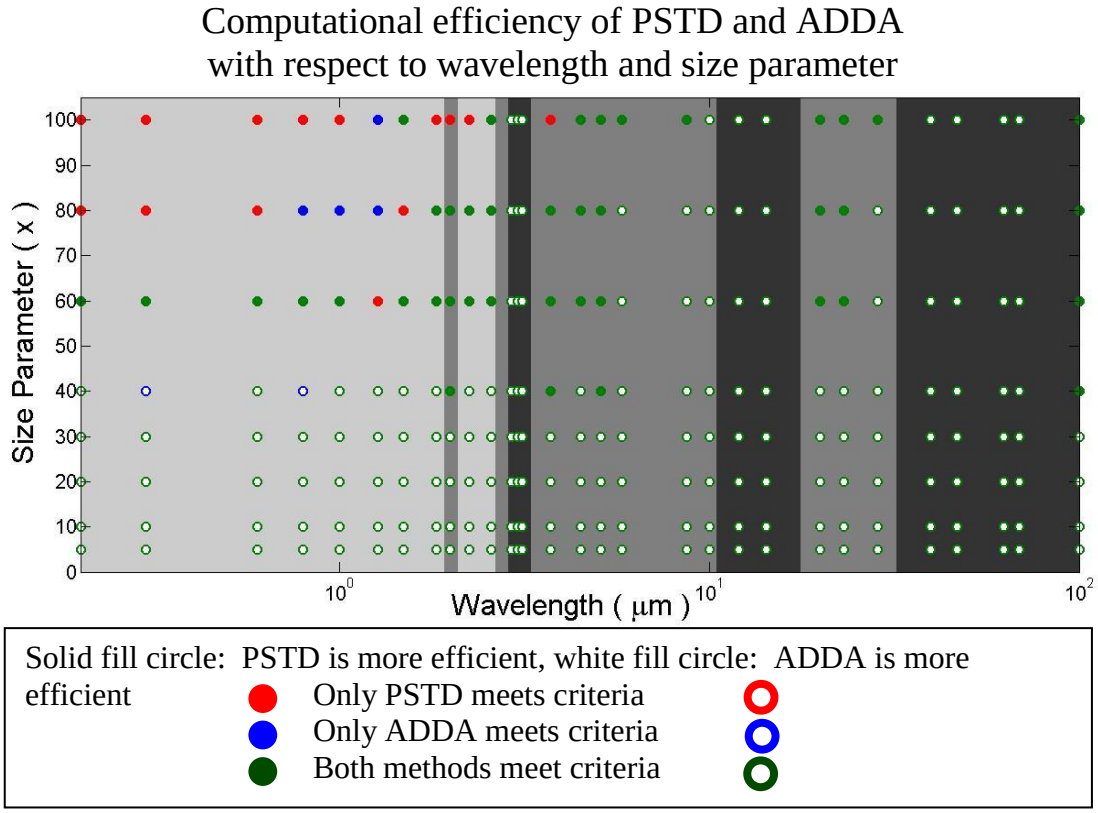

Figure 8 Computational efficiency and criteria validation of numerical methods.

Case 4, computational time (seconds) using 8 processors								
x	5	10	20	30	40	60	80	100
PSTD	43	209	1340	8866	8831	21807	80646	63818
ADDA	2	87	2130	6012	10641	87906	52817	53900

Table 4 Computational time results of the 8 size parameters for Case 4.

CHAPTER IV

CONCLUSION

Discussion

The purpose of this research was to expand the range of refractive indices measured to include absorptive cases and to systematically assess the accuracy and computational efficiency of the pseudo-spectral time domain (PSTD) and the discrete dipole approximation (DDA) methods in comparison to the Lorenz-Mie theory for a wide range of realistic refractive indices of atmospheric particles. The realistic refractive indices were applied to spherical particles because our analytical solution, Lorenz-Mie theory, is known for its capabilities in computing the single-scattering properties of spherical particles.

Assessing error calculations

We now refer back to Figure 3 to evaluate and compare the relative error (RE) and root mean squared relative error (RMSRE) for each method in the first 3 cases. The relative error averages, in Figure 3a, fluctuated with increasing size parameter in Cases 1 through 3 for PSTD and in Case 1 for ADDA. This was due to the variability in the input parameters. For Cases 2 and 3, the ADDA relative error averages decreased with increasing size parameter because the spatial resolution inputs for the two cases were similar at each of the size parameters. Figure 3b showed that as the size parameter increased, the RMSRE increased. The RMSRE increased at larger size parameters because the spatial resolution was decreased to compensate for the increase in computational time. The accuracy of the computations at large size parameters improved because the moderate size parameters (40-60) and larger size parameters used similar spatial resolutions.

Assessing phase matrices

In the results section, Figures 4 through 7 displayed the phase matrix elements and their corresponding errors for the 4 wavelength examples. Each example represented a different complex refractive index. Figures 4 through 6 presented the examples' results with respect to the size parameter, where Figure 4 was $x = 20$, Figure 5 was $x = 60$, and Figure 6 was $x = 100$. These three plots were formatted so that the left-side phase matrix elements were the results for a non-absorptive / weakly absorptive case (Case 1), the center phase matrix elements were the results for a moderately absorptive case (Case 2), and the right-side phase matrix elements were the results for a strongly absorptive case (Case 3). Figure 7 displayed the phase matrix elements and their errors for all 3 size parameters for the Case 4. Conclusions were drawn about the two methods' effectiveness at computing single-scattering properties by looking at the relative and absolute errors of the phase matrix elements in these figures.

For this study, $x = 20$ was considered a small size parameter. Figure 4 represented 3 sets of phase matrix elements for spherical particles with small size parameters. The ADDA simulations of the phase matrix elements of the non-absorptive and weakly absorptive cases became more variable as the functions approached the direct back-scattering angle (180^o). For the strongly absorptive case at $x = 20$, both the PSTD and ADDA simulations vary throughout the scattering angles.

The size parameter of 60 was considered a moderate size parameter for this study. Figure 5 represented 3 sets of phase matrix elements for spherical particles with moderate size parameters. The results showed that the relative errors of the PSTD and ADDA P_{11} phase functions varied more as they approached the direct backscattering angle (180^o) for the

non-absorptive case. The REs of PSTD and ADDA P_{11} phase functions for the moderately absorptive case varied more than the non-absorptive throughout all scattering angles, but ADDA was more variable than PSTD when approaching 180^o for this Case 2 example. The plot for the strongly absorptive case showed that the RE of the PSTD P_{11} phase function varied more than the ADDA P_{11} phase function in the forward scattering angles ($0\text{-}90^o$), but ADDA had a smaller RE than PSTD at 180^o for the strongly absorptive case.

Lastly, the phase matrix examples for a large size parameter were represented by the 3 Cases at $x = 100$. In Figure 6, the number of fluctuations of the phase matrix elements computed by the analytical solution and the 2 numerical methods were greater than the number of periodic fluctuations in the phase matrix elements of the examples at $x = 20$ and $x = 60$. For the non-absorptive / weakly absorptive case, PSTD and ADDA fluctuated with increasing amplitude as their P_{11} phase functions and phase ratios approached 180^o. For the weakly absorptive case, the errors in PSTD are smaller than ADDA and ADDA's errors along the scattering angles are periodic. At 0^o, the errors of the ADDA were minimal but increased as the scattering angles approached 45^o. The errors of ADDA also deflated between about 100^o and 135^o before they increased again closer to the direct back scattering angle. The errors for the strongly absorptive case at $x = 100$ varied throughout the scattering angles, similarly to the errors for the strongly absorptive case at $x = 20$ and $x = 60$.

Figure 7 brought together the analysis of the 3 size parameters for one specific case, Case 4. Case 4 differed from the other 3 cases due to the real part of its refractive index. The refractive index of Case 4 was 1.79, where as Cases 1 to3 was around 1.3 to 1.4. The variability of Case 4's PSTD and ADDA results for $x = 20$ were similar to the other 3 Cases at $x = 20$, so it was not easily discernible which method approximated the single-scattering

properties more effectively. For $x = 60$ and $x = 100$, the variability in the errors of the phase matrix elements decreased with increasing scattering angle toward direct back-scattering.

In all four examples, both PSTD and ADDA did a good job of approximating the Lorenz-Mie theory phase matrix elements for the strongly absorptive cases in comparison to the moderately absorptive, weakly absorptive, and non-absorptive cases. The oscillations in the phase functions increased with increasing size parameter and decreased with increasing imaginary refractive indices. However, it was not clear which numerical method did a better job of computing the single-scattering properties of spherical particles.

Assessing computational efficiencies of methods

As stated previously, the computational time was used to assess whether PSTD or ADDA was more efficient for computing single-scattering properties of spherical particles. Figure 8 and Table 4 showed the computational time results for the 31 wavelengths at each of the 8 size parameters. Figure 8 demonstrated whether PSTD or ADDA was efficient at computing the single-scattering properties. Figure 8 also showed whether a method met the criteria stated in Methodology, where the relative error of the extinction efficiency was less than or equal to 2% and the root mean squared relative error of the P_{11} phase function was less than or equal to 30%. Most of the data met both criteria, but for some of the data at larger size parameters, only one of the methods met the set criteria.

The wavelengths in the visible to near infrared ranges had refractive indices that were non-absorptive to weakly absorptive. For the non-absorptive / weakly absorptive cases, it was found that PSTD was more efficient at computing the single-scattering properties than ADDA at size parameters greater than about 50. The infrared to microwave wavelength ranges contained both moderately and strongly absorptive cases. For moderately absorptive

cases, it was found that ADDA was more efficient than PSTD for size parameters less than 60. The size parameter at which PSTD was more efficient varied from 60 to 80 in the infrared wavelength range. For the strongly absorptive cases, ADDA was more efficient at all size parameters from 5 to 100.

Summary

The goals of this study were to further test and understand the capabilities of PSTD and ADDA numerical methods in computing single-scattering properties of atmospheric particles. Most particles in the atmosphere are non-spherical. In order to measure the accuracies of the two methods with respect to the Lorenz-Mie theory, spherical particles were used in the study. Both the PSTD method and the ADDA method efficiently computed the single-scattering properties for spherical particles within the prescribed accuracy criteria when compared to the Lorenz-Mie theory. From this study, it was found that the efficiencies of the two methods did not only depend on the real part of the refractive indices, but also depended on the imaginary part of the refractive indices. Although the focus of this study was on atmospheric particles, the numerical analysis can be applied to biological particles. Further studies will need to be done to continue refining the accuracy criteria and the spatial resolutions for each method.

REFERENCES

Chen, G. Modeling of the optical properties of nonspherical particles in the atmosphere. PhD Dissertation, Texas A&M University, College Station, TX. 2007.

Hesthaven, J., Gottlieb, S. & Gottlieb, D. Spectral Methods for Time-Dependent Problems. Cambridge University Press, New York, NY. 2007.

Liou K. N. An Introduction to Atmospheric Radiation. Academic Press, San Diego, CA. 2002.

Liu, C, et al. Application of the pseudo-spectral time domain method to compute particle single-scattering properties from size parameters up to 200. J. Quant. Spectrosc. Radiat. Transfer. 2012a; 113: 1728-1740.

Liu, C., et al. Comparison between the pseudo-spectral time domain method and the discrete dipole approximation for light scattering simulations. Opt. Express. 2012b; 20: 16763-16776.

Mie, G. Beitrage zur optic truber medien, speziell kolloidaler metallosungen. Ann. d. Phys. 1908; 25: 337-445.

Thomas, G. and Stamnes, K. Radiative Transfer in the Amphere and Ocean. Cambridge University Press, New York, NY. 1999.

Van du Hulst, H.C. Light Scattering by Small Particles. Dover Publications, Inc., New York, NY. 1981.

Warren, S. G. and Brandt, R. E. Optical constants of ice from the ultraviolet to the microwave: A revised compilation. J. Geophys. Res. 2008; 113: D14220, http://dx.doi.org/10.1029/2007JD009744.

Yang, P. and Liou, K.N. Finite-difference time domain method for light scattering by small ice crystals in three-dimensional space J.Opt Soc. Am. 1996; 13: 2072-2085.

Yang, P. and Liou, K. N. Finite difference time domain method for light scattering by nonspherical particles. In Mishchenko, M. I., Hovenier, J. W., and Travis L. D. Light Scattering by Nonspherical Particles: Theory, Measurements, and Geophysical Applications. San Diego, CA: Academic Press, 2000; pgs. 173-221.

Yurkin, M. A., et al. Systematic comparison of the discrete dipole approximation and the finite difference time domain method for large dielectric scatterers. Opt. Express. 2007; 15: 17902-17911.

Yurkin, M. A. and Hoekstra, A. G. User Manual for Discrete Dipole Approximation Code ADDA v. 0.79. Creative Commons, San Francisco, CA, 2009. http://a-dda.goodlecode.com/svn/tags/rel_0_79/doc/manuel.pdf.

Yurkin, M. A. and Hoekstra, A. G. The discrete-dipole-approximation code ADDA: Capabilities and know limitations. J. Quant. Spectrosc. Radiat. Transfer 2011; 112: 2234-2247.

APPENDIX

Time results (in seconds) of PSTD and ADDA simulations (8 parallel processors)																	
Size Parameter (x)		5		10		20		30		40		60		80		100	
Case #	WL	PSTD	ADDA	PSTD	ADDA	PSTD	ADDA	PSTD	ADDA	PSTD	ADDA	PSTD	ADDA	PSTD	ADDA	PSTD	ADDA
Case 1	1	37	2	226	3	1279	189	8401	1933	13393	3136	20486	153081	43347	29145	57725	30892
	2	40	2	271	3	2052	112	8019	1300	55223	42058	26105	27452	40035	98435	57783	0
	4	63	2	323	3	1038	83	5465	987	6667	4769	54793	73973	59559	57335	47594	154076
	5	38	3	322	2	4151	82	19790	1009	76068	62212	16364	21645	47396	113322	123256	0
	6	37	2	322	3	1715	77	10312	2043	6680	3861	16189	17986	124739	127791	22845	88713
	7	35	2	318	2	1028	68	22720	972	6551	3813	31750	49102	102019	153407	132001	83476
	8	36	1	189	3	1021	54	6705	722	6478	5839	16240	25379	34002	109147	46600	148650
	9	35	1	523	3	1023	50	22318	644	6485	3325	16022	17556	58718	69540	45970	128801
	11	35	2	157	3	1008	38	18863	492	6164	2622	24535	52582	9625	88280	46037	79669
	12	33	1	157	2	961	22	6033	205	5986	1101	8397	8671	12599	15279	43567	62936
Case 2	10	35	2	163	7	1013	47	18990	486	2140	3117	4741	11439	10111	22724	46469	62883
	18	41	2	45	8	363	129	5325	779	1683	3861	3650	10986	4272	53112	5662	171796
	19	25	2	167	5	354	45	1701	264	1638	929	2084	2630	4002	4405	5574	11625
	20	25	2	82	5	244	67	1677	529	1629	1668	2089	5005	3986	11196	5532	37464
	21	25	2	51	4	351	28	1639	157	1600	508	2018	1593	4026	2910	5272	6144
	23	25	2	51	8	348	28	1633	162	1584	541	2001	1763	4009	2996	5257	6817
	24	25	2	49	5	510	13	1541	62	1490	187	1910	646	3815	1106	4929	2410
	29	26	2	54	14	783	57	1818	375	1764	1170	2241	3749	4545	4638	6021	8442
	30	44	2	176	15	254	94	1770	540	1716	1662	2144	4945	4337	37067	5775	57650
	31	43	3	52	8	245	35	3532	177	1633	662	2044	1913	3983	3363	5515	7867
Case 3	13	20	2	38	3	156	8	898	33	840	90	1656	214	3108	324	4187	668
	14	24	2	39	6	165	15	972	62	915	175	1817	459	3513	745	4747	1626
	16	22	2	89	7	184	23	1141	98	1089	260	2248	815	4480	1109	5981	2845
	26	25	2	41	3	363	15	1044	63	996	177	2005	478	3995	748	5257	1631
	27	45	2	108	11	401	31	1177	132	1127	460	2348	1252	4731	1725	6326	3917
	32	43	2	40	9	169	12	1012	52	964	140	1939	385	3772	614	5111	1331
	34	43	2	41	14	176	21	1071	97	1021	291	2070	877	4014	1125	5489	3014
	37	46	2	47	18	404	29	1206	127	1162	440	2397	1077	4858	1721	6458	3868
	38	55	2	48	23	421	35	1260	169	1199	496	2481	1358	5085	2049	6753	4163
	40	48	6	32	42	436	87	1305	474	1260	1449	2649	2788	3084	4478	7303	9809
Case 4	41	43	2	209	87	1340	2130	8866	6012	8831	10641	21807	87906	80646	52817	63818	53900

Table A1 Computational time for PSTD and ADDA at x = {5, 10, 20, 30, 40, 60, 80, 100}.

Relative Errors of Extinction Efficiency results of PSTD and ADDA simulations																	
(x)		5		10		20		30		40		60		80		100	
#	WL	PSTD	ADDA	PSTD	ADDA	PSTD	ADDA	PSTD	ADDA	PSTD	ADDA	PSTD	ADDA	PSTD	ADDA	PSTD	ADDA
1	1	3.4(-3)	5.3(-3)	-6.3(-5)	5.5(-3)	1.6(-2)	-8.4(-3)	-1.6(-3)	-1.0(-2)	6.9(-3)	1.4(-2)	-2.2(-3)	2.0(-2)	9.9(-3)	-4.6(-3)	1.1(-2)	4.7(-2)
	2	2.2(-3)	2.3(-3)	7.6(-3)	6.0(-3)	3.5(-3)	1.2(-3)	1.1(-3)	3.8(-3)	-4.4(-2)	-4.3(-2)	-2.6(-3)	1.4(-2)	-8.6(-3)	1.9(-2)	-5.2(-3)	-
	4	-1.5(-3)	1.1(-3)	6.7(-3)	4.3(-3)	-2.8(-3)	6.9(-3)	-5.7(-3)	-1.3(-3)	4.8(-3)	1.0(-3)	1.2(-2)	7.2(-3)	1.6(-2)	-1.1(-2)	-3.4(-3)	3.4(-3)
	5	1.5(-3)	9.3(-4)	6.4(-3)	3.6(-3)	-8.5(-3)	-8.3(-3)	-8.4(-3)	1.7(-3)	-3.7(-2)	-1.9(-2)	7.5(-3)	-1.8(-5)	-9.3(-3)	-1.6(-3)	9.1(-3)	-
	6	1.4(-3)	8.2(-4)	6.3(-3)	3.1(-3)	-9.5(-3)	-1.1(-2)	5.3(-3)	1.3(-2)	1.3(-3)	2.6(-3)	-8.0(-4)	-4.4(-3)	-3.6(-3)	5.3(-3)	5.5(-3)	5.8(-3)
	7	1.3(-3)	6.7(-4)	6.5(-3)	2.7(-3)	4.1(-3)	-4.8(-3)	1.2(-3)	-5.3(-3)	3.7(-3)	1.3(-3)	-1.6(-2)	-2.6(-2)	-4.3(-3)	5.4(-3)	1.7(-2)	2.3(-2)
	8	1.2(-3)	5.5(-4)	7.4(-3)	2.2(-3)	6.8(-3)	8.4(-5)	6.0(-4)	1.1(-3)	-3.7(-3)	4.9(-3)	1.7(-3)	9.4(-3)	1.8(-2)	-4.0(-3)	-1.3(-2)	4.1(-3)
	9	8.4(-4)	2.0(-4)	6.8(-3)	6.6(-4)	-4.0(-4)	9.8(-4)	-3.5(-3)	3.2(-3)	-5.7(-3)	-2.0(-4)	-3.3(-3)	3.3(-3)	1.2(-2)	9.1(-4)	-6.5(-3)	-1.1(-3)
	11	1.4(-4)	-1.7(-4)	5.7(-3)	-7.2(-5)	3.4(-3)	2.2(-3)	-1.4(-2)	8.4(-4)	-6.0(-3)	-4.6(-4)	1.2(-2)	1.4(-3)	2.7(-3)	-1.6(-3)	-1.0(-2)	7.0(-3)
	12	-1.6(-3)	-1.7(-4)	4.2(-3)	-4.4(-4)	-4.8(-4)	9.6(-4)	-3.1(-3)	-1.6(-3)	-5.0(-3)	-2.4(-3)	3.1(-3)	-6.5(-3)	5.5(-3)	4.6(-3)	-1.3(-2)	8.7(-4)
2	10	6.6(-4)	1.0(-4)	6.7(-3)	9.4(-4)	-2.4(-3)	2.8(-4)	-5.5(-3)	-2.3(-3)	-6.8(-3)	-3.8(-3)	2.2(-3)	-1.7(-3)	1.2(-2)	-3.5(-3)	-1.4(-2)	-3.1(-3)
	18	2.6(-3)	1.9(-3)	2.4(-3)	-1.0(-4)	6.8(-4)	-2.6(-3)	4.6(-3)	-2.7(-3)	6.3(-3)	3.1(-3)	2.1(-3)	4.3(-3)	3.7(-3)	4.6(-4)	3.1(-3)	2.5(-3)
	19	1.6(-3)	1.5(-3)	5.8(-3)	2.4(-3)	4.7(-3)	1.1(-3)	3.3(-3)	7.7(-4)	8.8(-4)	4.7(-4)	5.0(-3)	3.6(-4)	5.3(-4)	2.5(-4)	3.1(-3)	2.1(-4)
	20	-6.0(-4)	8.3(-4)	8.6(-3)	2.9(-3)	-1.2(-3)	2.1(-3)	2.7(-3)	8.6(-4)	1.7(-3)	3.1(-4)	3.8(-3)	6.5(-5)	-6.1(-5)	4.6(-4)	4.1(-3)	1.9(-4)
	21	1.1(-3)	9.0(-4)	3.8(-3)	1.8(-3)	6.0(-3)	6.2(-4)	3.5(-3)	5.1(-4)	1.6(-3)	4.2(-4)	5.0(-3)	2.3(-4)	5.5(-5)	1.7(-4)	3.8(-3)	1.3(-4)
	23	8.6(-4)	7.8(-4)	4.6(-3)	1.3(-3)	5.9(-3)	6.2(-4)	3.4(-3)	4.1(-4)	1.3(-3)	2.3(-4)	4.3(-3)	2.6(-4)	-5.3(-4)	1.4(-4)	3.2(-3)	9.7(-5)
	24	4.0(-4)	2.1(-4)	3.5(-3)	2.4(-4)	3.1(-3)	2.0(-4)	4.3(-3)	-6.5(-5)	2.3(-3)	-7.1(-5)	6.4(-3)	4.5(-7)	1.7(-3)	7.2(-5)	3.6(-3)	2.4(-5)
	29	6.0(-3)	3.0(-3)	2.0(-3)	1.7(-3)	2.5(-3)	1.6(-3)	3.5(-3)	1.0(-3)	1.2(-3)	6.2(-4)	5.0(-3)	5.0(-4)	7.7(-5)	4.2(-4)	3.3(-3)	2.9(-4)
	30	7.6(-3)	1.7(-3)	5.3(-3)	2.7(-3)	3.4(-3)	9.9(-4)	3.4(-3)	3.2(-4)	3.5(-4)	5.0(-4)	4.5(-3)	5.8(-4)	-2.5(-4)	3.0(-4)	3.5(-3)	2.8(-4)
	31	-3.0(-4)	1.5(-3)	5.9(-3)	1.9(-3)	5.2(-3)	6.7(-4)	3.4(-3)	7.7(-4)	1.3(-3)	3.8(-4)	4.8(-3)	2.3(-4)	9.3(-4)	2.2(-4)	3.2(-3)	1.6(-4)
3	13	3.5(-3)	-4.0(-4)	1.7(-3)	1.1(-4)	1.9(-5)	-1.6(-4)	1.7(-4)	-1.8(-4)	-6.8(-4)	-2.3(-4)	4.9(-3)	-5.7(-5)	-5.0(-4)	-2.0(-4)	1.3(-3)	-3.2(-4)
	14	3.4(-3)	-2.2(-3)	-4.9(-5)	-1.4(-3)	3.7(-3)	-1.2(-3)	4.1(-3)	-8.9(-4)	-1.2(-3)	-8.4(-4)	1.4(-3)	-5.0(-4)	-1.6(-3)	-4.7(-4)	2.3(-3)	-4.5(-4)
	16	7.6(-3)	1.6(-3)	4.7(-3)	1.3(-4)	4.5(-3)	-1.0(-4)	3.7(-3)	-2.4(-4)	3.2(-4)	-1.9(-4)	4.4(-3)	-2.3(-4)	2.6(-4)	-2.7(-4)	2.3(-3)	-2.6(-4)
	26	5.6(-3)	7.8(-5)	3.8(-3)	-1.1(-4)	1.8(-3)	-4.6(-4)	2.0(-3)	-1.6(-4)	1.4(-4)	-4.6(-5)	2.6(-3)	-2.4(-4)	-7.3(-4)	-2.5(-4)	3.1(-3)	-2.0(-4)
	27	6.5(-3)	3.5(-3)	4.8(-3)	1.9(-3)	2.7(-3)	1.4(-3)	3.4(-3)	9.3(-4)	1.2(-3)	5.6(-4)	3.6(-3)	3.7(-4)	-1.6(-4)	3.1(-4)	3.5(-3)	1.8(-4)
	32	2.4(-3)	4.8(-4)	4.2(-3)	9.2(-5)	2.4(-3)	3.8(-5)	4.9(-3)	1.7(-4)	3.5(-3)	-6.5(-5)	2.9(-3)	-9.8(-5)	1.2(-3)	-5.2(-5)	2.6(-3)	-1.2(-4)
	34	2.4(-3)	-3.0(-3)	9.9(-4)	-1.8(-3)	1.8(-3)	-2.4(-3)	8.4(-4)	-1.6(-3)	-1.1(-3)	-1.3(-3)	3.6(-3)	-1.2(-3)	-1.2(-3)	-9.4(-4)	1.1(-3)	-7.6(-4)
	37	7.1(-3)	4.2(-3)	4.4(-3)	1.9(-3)	2.7(-3)	1.3(-3)	3.9(-3)	8.1(-4)	1.0(-3)	4.9(-4)	4.3(-3)	2.9(-4)	4.5(-4)	1.9(-4)	3.4(-3)	1.1(-4)
	38	8.4(-3)	5.6(-3)	5.7(-3)	2.2(-3)	2.9(-3)	1.7(-3)	4.3(-3)	9.9(-4)	2.3(-3)	6.0(-4)	4.6(-3)	3.2(-4)	3.1(-4)	2.1(-4)	3.7(-3)	1.1(-4)
	40	3.8(-3)	5.4(-3)	6.3(-3)	3.6(-3)	3.6(-3)	3.1(-3)	4.5(-3)	2.0(-3)	2.0(-3)	1.4(-3)	4.7(-3)	1.0(-3)	2.7(-3)	8.2(-4)	4.3(-3)	5.9(-4)
4	41	-1.5(-2)	-1.9(-2)	4.8(-3)	1.5(-2)	-8.0(-4)	-3.5(-3)	-4.5(-3)	-2.0(-3)	-7.1(-4)	-2.0(-3)	3.1(-3)	-5.5(-4)	1.2(-2)	-6.4(-4)	-1.1(-2)	8.3(-3)

Table A2 Relative errors of the extinction efficiency for PSTD and ADDA.

Root Mean Squared relative error for size parameters of PSTD and ADDA simulations																	
(x)		5		10		20		30		40		60		80		100	
#	WL	PSTD	ADDA	PSTD	ADDA	PSTD	ADDA	PSTD	ADDA	PSTD	ADDA	PSTD	ADDA	PSTD	ADDA	PSTD	ADDA
1	1	8.2(-3)	7.2(-2)	6.3(-2)	1.5(-1)	1.8(-1)	1.5(-1)	1.3(-1)	1.2(-1)	2.4(-1)	1.7(-1)	1.7(-1)	2.8(-1)	2.1(-1)	4.3(0)	2.4(-1)	5.9(0)
	2	9.4(-3)	5.8(-2)	1.7(-2)	4.2(-2)	1.2(-1)	6.3(-2)	1.3(-1)	6.5(-2)	3.9(-1)	3.8(-1)	1.9(-1)	2.8(-1)	1.7(-1)	3.1(-1)	2.9(-1)	-
	4	1.6(-2)	4.7(-2)	2.7(-2)	5.0(-2)	1.5(-1)	9.3(-2)	1.2(-1)	6.7(-2)	7.2(-2)	6.5(-2)	2.6(-1)	2.8(-1)	2.1(-1)	4.8(-1)	2.4(-1)	4.0(-1)
	5	1.0(-2)	4.5(-2)	2.3(-2)	5.1(-2)	1.3(-1)	1.0(-1)	1.6(-1)	7.7(-2)	8.8(-1)	1.7(0)	1.7(-1)	1.8(-1)	3.5(-1)	4.2(-1)	2.2(-1)	-
	6	1.1(-2)	4.4(-2)	2.1(-2)	5.3(-2)	1.2(-1)	1.0(-1)	2.2(-1)	1.8(-1)	1.0(-1)	8.9(-2)	1.7(-1)	1.9(-1)	8.9(-1)	7.9(-1)	2.7(-1)	3.7(0)
	7	1.1(-2)	4.3(-2)	1.9(-2)	5.5(-2)	1.6(-1)	1.0(-1)	1.9(-1)	1.2(-1)	8.7(-2)	7.7(-2)	2.6(-1)	3.5(-1)	3.3(-1)	1.2(0)	4.5(-1)	2.0(0)
	8	1.1(-2)	4.1(-2)	1.6(-2)	5.7(-2)	9.1(-2)	6.9(-2)	1.6(-1)	5.5(-2)	1.3(-1)	1.4(-1)	1.6(-1)	1.7(-1)	2.8(-1)	4.2(-1)	2.0(-1)	2.8(-1)
	9	1.1(-2)	3.9(-2)	1.8(-2)	6.3(-2)	7.9(-2)	5.2(-2)	1.0(-1)	9.3(-2)	2.0(-1)	7.3(-2)	2.0(-1)	1.5(-1)	2.3(-1)	2.9(-1)	2.7(-1)	4.7(-1)
	11	1.1(-2)	3.5(-2)	2.3(-2)	7.5(-2)	5.5(-2)	4.5(-2)	1.5(-1)	1.4(-1)	1.3(-1)	6.6(-2)	2.8(-1)	2.0(-1)	2.9(-1)	2.5(-1)	3.0(-1)	3.2(-1)
	12	1.2(-2)	3.5(-2)	1.9(-2)	5.0(-2)	2.7(-2)	4.0(-2)	5.7(-2)	4.3(-2)	1.3(-1)	6.2(-2)	1.8(-1)	1.4(-1)	3.0(-1)	1.0(-1)	1.5(-1)	1.5(-1)
2	10	1.1(-2)	1.4(-2)	1.9(-2)	2.2(-2)	6.6(-2)	4.4(-2)	6.5(-2)	7.5(-2)	2.0(-1)	1.3(-1)	2.0(-1)	2.0(-1)	2.1(-1)	2.6(-1)	1.8(-1)	3.7(-1)
	18	3.1(-2)	2.1(-2)	1.8(-1)	3.4(-2)	9.2(-2)	1.1(-1)	2.4(-1)	1.0(-1)	2.1(-1)	1.6(-1)	1.2(-1)	2.6(-1)	2.5(-1)	3.0(-1)	2.1(-1)	3.6(-1)
	19	1.6(-2)	2.3(-2)	1.6(-2)	2.1(-2)	5.6(-2)	6.4(-2)	3.2(-2)	7.1(-2)	4.0(-2)	5.4(-2)	5.5(-2)	6.6(-2)	6.7(-2)	9.1(-2)	1.0(-1)	1.3(-1)
	20	1.4(-2)	1.8(-2)	1.7(-2)	2.6(-2)	1.5(-1)	6.0(-2)	1.6(-1)	8.4(-2)	1.2(-1)	8.4(-2)	1.9(-1)	1.5(-1)	1.2(-1)	1.7(-1)	1.2(-1)	1.8(-1)
	21	1.0(-2)	1.5(-2)	2.9(-2)	3.3(-2)	4.6(-2)	6.3(-2)	2.4(-2)	7.2(-2)	3.6(-2)	5.1(-2)	5.6(-2)	6.4(-2)	7.1(-2)	9.3(-2)	1.2(-1)	1.3(-1)
	23	1.0(-2)	1.5(-2)	3.1(-2)	2.3(-2)	4.5(-2)	6.0(-2)	3.3(-2)	6.9(-2)	3.8(-2)	4.9(-2)	6.5(-2)	6.6(-2)	7.6(-2)	9.3(-2)	1.0(-1)	1.3(-1)
	24	2.3(-2)	1.7(-2)	7.8(-2)	3.5(-2)	3.5(-2)	6.0(-2)	3.3(-2)	7.4(-2)	3.8(-2)	5.9(-2)	5.4(-2)	6.7(-2)	7.0(-2)	9.7(-2)	1.0(-1)	1.4(-1)
	29	3.8(-2)	3.2(-2)	3.5(-2)	3.4(-2)	2.2(-2)	8.6(-2)	2.2(-2)	7.3(-2)	3.5(-2)	4.7(-2)	5.6(-2)	6.3(-2)	6.8(-2)	8.6(-2)	1.1(-1)	1.3(-1)
	30	3.4(-2)	1.0(-2)	2.7(-2)	2.6(-2)	7.7(-2)	8.8(-2)	4.3(-2)	9.2(-2)	4.2(-2)	1.2(-1)	6.8(-2)	7.0(-2)	6.9(-2)	9.1(-2)	1.1(-1)	1.3(-1)
	31	4.6(-2)	2.2(-2)	2.2(-2)	2.3(-2)	6.1(-2)	8.8(-2)	2.2(-2)	7.2(-2)	3.5(-2)	4.8(-2)	5.4(-2)	6.4(-2)	6.4(-2)	9.1(-2)	9.5(-2)	1.3(-1)
3	13	5.4(-2)	1.9(-2)	9.3(-2)	3.6(-2)	5.7(-2)	5.8(-2)	3.9(-2)	6.9(-2)	4.3(-2)	4.3(-2)	6.5(-2)	5.9(-2)	6.5(-2)	8.8(-2)	1.0(-1)	1.2(-1)
	14	3.3(-2)	2.2(-2)	6.1(-2)	3.1(-2)	5.8(-2)	5.3(-2)	4.0(-2)	6.0(-2)	4.7(-2)	4.3(-2)	8.1(-2)	5.6(-2)	7.4(-2)	7.7(-2)	1.1(-1)	1.2(-1)
	16	4.6(-2)	3.4(-2)	4.4(-2)	3.4(-2)	5.9(-2)	5.9(-2)	2.9(-2)	6.4(-2)	5.0(-2)	4.6(-2)	6.2(-2)	6.1(-2)	6.7(-2)	8.3(-2)	1.1(-1)	1.3(-1)
	26	3.4(-2)	2.7(-2)	2.7(-2)	3.8(-2)	2.7(-2)	5.9(-2)	4.2(-2)	6.4(-2)	5.5(-2)	4.5(-2)	8.8(-2)	5.8(-2)	6.6(-2)	8.2(-2)	9.8(-2)	1.3(-1)
	27	2.0(-2)	3.6(-2)	3.1(-2)	3.3(-2)	2.5(-2)	6.4(-2)	2.3(-2)	6.7(-2)	4.3(-2)	4.6(-2)	7.7(-2)	6.1(-2)	6.7(-2)	8.3(-2)	1.0(-1)	1.3(-1)
	32	2.5(-2)	2.4(-2)	3.6(-2)	1.2(-2)	3.8(-2)	6.3(-2)	4.5(-2)	6.7(-2)	4.1(-2)	4.5(-2)	8.9(-2)	5.9(-2)	6.4(-2)	8.5(-2)	1.0(-1)	1.3(-1)
	34	2.3(-2)	2.9(-2)	4.0(-2)	1.7(-2)	5.9(-2)	5.5(-2)	3.8(-2)	6.2(-2)	5.0(-2)	4.8(-2)	6.7(-2)	6.2(-2)	7.3(-2)	8.0(-2)	1.2(-1)	1.3(-1)
	37	2.3(-2)	4.0(-2)	4.1(-2)	1.3(-2)	3.0(-2)	6.3(-2)	3.0(-2)	6.6(-2)	4.5(-2)	4.7(-2)	6.5(-2)	6.2(-2)	6.4(-2)	8.3(-2)	1.0(-1)	1.3(-1)
	38	2.5(-2)	4.4(-2)	4.4(-2)	1.8(-2)	2.4(-2)	6.3(-2)	2.9(-2)	6.6(-2)	4.3(-2)	4.8(-2)	6.1(-2)	6.3(-2)	6.4(-2)	8.4(-2)	1.2(-1)	1.4(-1)
	40	3.5(-2)	3.2(-2)	4.5(-2)	2.3(-2)	2.5(-2)	6.9(-2)	2.3(-2)	6.9(-2)	3.9(-2)	5.1(-2)	6.8(-2)	6.5(-2)	1.0(-1)	8.2(-2)	1.2(-1)	1.4(-1)
4	41	5.4(-2)	1.9(-1)	2.9(-2)	1.5(-1)	8.2(-2)	2.0(-1)	7.0(-2)	2.4(-1)	9.4(-2)	4.2(-1)	2.4(-1)	6.8(-1)	2.4(-1)	4.6(-1)	1.3(-1)	7.0(-1)

Table A3 Root mean squared relative errors of the P_{11} phase functions for PSTD and ADDA.